Cooperative radiative dynamics in molecular aggregates

Francis C. Spano,[a] Jan R. Kuklinski, and Shaul Mukamel[b]
University of Rochester, Chemistry Department, Rochester, New York 14627

(Received 17 July 1990; accepted 18 January 1991)

We theoretically investigate the radiative dynamics of molecular aggregates with physical dimensions much smaller than an optical wavelength. The fluorescence decay rate of a one-dimensional aggregate consisting of N electronically coupled two-level molecules interacting with acoustic and optical lattice phonons is calculated. The linear dependence (superradiance) of the radiative decay rate on the aggregate size N is shown to be quenched by exciton–phonon coupling. An increase of aggregate size N eventually leads to a convergent, size independent decay rate, which is N^* times faster than the monomer decay rate. The *coherence size* N^* is generally a function of the exciton–phonon coupling strength, the phonon bandwidth, and the aggregate temperature. For low frequency phonons, a scaling law is obtained and an empirical relation for the temperature dependence $N^* \sim T^{-1/3}$ is derived.

I. INTRODUCTION

The excited state dynamics of aggregated molecules is a subject of increasing interest. Molecular aggregates function in such diverse roles as sensitizers in color photography,[1] and energy transport media in natural photosynthetic systems.[2] Recently, the nonlinear optical properties of interacting molecules arranged in an aggregate have received considerable theoretical attention,[3-5] in an attempt to appraise their value as potential nonlinear optical materials useful for opto-electronic devices. It is natural to interpret the optical response of molecular aggregates in terms of a characteristic *coherence size*. Molecules located within the coherence size are closely coupled and respond in phase to the external field. This may result in ultrafast radiative decay rates and enhanced optical nonlinearities. It is the possibility of maintaining a large coherence size which makes the studies of molecular aggregates particularly exciting.

The radiative dynamics of J aggregates, formed by many types of dye molecules (e.g., pseudo-isocyanine dyes), have been extensively studied.[6,7] For these systems, the concept of a coherence size was first advanced by Mobius and Kuhn[6(a)] in analyzing the dependence of fluorescence quenching on the acceptor surface density for a system consisting of an acceptor monolayer on top of a J-aggregate monolayer. Additional experiments,[6(b)] where the acceptor impurity was incorporated into the J-aggregate monolayer, provided further evidence. The coherence size was found to be inversely proportional to the temperature for temperatures exceeding about 20 K [coherence size $= 3000/T(\mathrm{K})$]. deBoer and Wiersma[7] have also found an approximate inverse relationship between the size and the temperature above ~ 50 K. A similar size-dependent radiative decay rate has been observed from Wannier excitons in semiconductor microstructures, such as quantum dots and wells, and from charge transfer excitons in polysilanes.[8] Itoh and coworkers[9] have shown that spherical microcrystallites of CuCl embedded in a sodium chloride pellet radiate at a rate roughly proportional to the crystallite volume. The temperature dependence of the fluorescence lifetime of free excitons in quantum wells has been studied by Feldman *et al.*[10] and by Minami *et al.*,[11] where a nonactivated and approximately linear dependence was observed. A crude model for the temperature-dependent exciton coherence volume, determined by the strength of acoustic photon–exciton interaction, was used to rationalize that linear dependence.

In this article we develop a microscopic theory for the coherence size which determines the cooperative radiative decay of molecular aggregates. Most earlier theories of aggregate spectroscopy deal exclusively with the effects of aggregation on the monomer vibronic spectrum and include only the high frequency intramolecular vibrations, which show up in the optical spectra.[12-16] The radiative decay is, however, primarily influenced by the low frequency intermolecular vibrations or lattice photons, which have not received much theoretical attention. The coherence size for the radiative decay rate was calculated by Grad *et al.*[17] using a stochastic (infinite temperature) Haken–Strobl model.[18] It was shown that superradiance is quenched by homogeneous dephasing. The variation of the coherence size from $(\lambda/a)^d$ (a = lattice constant, d = dimensionality) for an infinite aggregate with no dephasing, to unity for large dephasing was shown. Spano and Mukamel[19] calculated the effect of static inhomogeneous broadening on the radiative lifetime of rigid aggregates, and showed that the coherence size is reduced to one when $\sigma/|V| \gg 1$, where σ is the width of the inhomogeneously broadened transition and $\hbar V$ is the intermolecular dipole–dipole coupling energy. In this paper, the coherence domain hypothesis is investigated by performing numerical simulations of the radiation dynamics for a one-dimensional aggregate with acoustic and optical exciton-phonon coupling. Our approach is microscopic and provides a finite temperature theory for phonon dephasing, an improvement over the popular and readily applicable Haken–Strobl model,[18] which cannot adequately explain the increase in fluorescence lifetime with temperature.[17] We derive reduced equations of motion in k space for the N exciton populations using a factorization procedure developed by Bogolyubov and Tyablikov.[20] It amounts to truncating the infinite hierarchy of equations for exciton–phonon operators by factorizing the expectation value of an exciton–photon product operator into the product of expectation values of

[a] Current address, Dept. of Chemistry, Temple University, Philadelphia, PA 19122.
[b] Camille and Henry Dreyfus Teacher/Scholar.

 0021-9606/91/117534-11$03.00

the exciton and the phonon parts. The same procedure has been used to calculate the absorption spectrum[21] (without the inclusion of superradiance) where factorization at the nth level corresponds to an nth-order perturbation treatment of the self-energy. Within this framework, we study the dependence of the fluorescence lifetime on the aggregate size N, the temperature, and the strength of the exciton–phonon coupling.

In Sec.II we present the model Hamiltonian including the electronic and nuclear degrees of freedom as well as the exciton–phonon coupling. In Sec. III we derive reduced equations of motion for the exciton populations and in Sec. IV we calculate the effects of phonon dephasing (acoustic and optical) and superradiance on the aggregate radiative rate for aggregates as large as $N = 400$. (Details of our calculations are given in the appendices.) Section V compares our results with those using a strong collision model which includes the Haken–Strobl model as a limiting case. Our conclusions, which provide a qualitative interpretation to the recent studies in semiconductors and J aggregates, are summarized in Sec. VI.

II. MODEL HAMILTONIAN

The aggregate is modeled as a cyclic array of N coupled two-level molecules with optical transition frequency ω_0.[4,22] The molecules interact via an oscillating electronic transition dipole moment μ between the ground state $|g\rangle$ and excited state $|e\rangle$. It is assumed that in the rigid lattice the dipole moments of all molecules are aligned and form an equilibrium angle θ_{12} with the aggregate axis. The equilibrium nearest-neighbor distance is r_{12}. At equilibrium, the values of θ and r are at the minimum of the molecular rotation and displacement potential wells, respectively. We further assume that the aggregate size is much smaller than an optical wavelength, note that inhomogenious broadening, which is neglected here, may provide an additional important mechanism for controlling the coherence size.[19]

In the rigid lattice, the coupling of the molecular transition dipole moments via the oscillating dipole electric field leads to the familiar exciton eigenstates. The complete Hamiltonian which includes the coupled two-level electronic states (excitons), the phonon field, and the interaction between the excitations and the phonons is written as

$$H = H_e + H_p + H_{ep}, \tag{2.1}$$

where

$$H_e = \hbar \sum_{k=0}^{N-1} \left\{ \omega(k) + i \frac{\gamma(k)}{2} \right\} B_k^\dagger B_k, \tag{2.2a}$$

$$H_p = \hbar \sum_s \sum_{q=0}^{N-1} \Omega_s(q) \left\{ b_{qs}^\dagger b_{qs} + \frac{1}{2} \right\}, \tag{2.2b}$$

$$H_{ep} = \frac{\hbar}{\sqrt{N}} \sum_{s,k,q} F_s(k,q) B_{k+q}^\dagger B_k (b_{q,s} + b_{N-q,s}^\dagger). \tag{2.2c}$$

(From here on, we set $\hbar = 1$, so that energy has units of s^{-1}.) The aggregate Hamiltonian includes site–off diagonal exciton–phonon coupling, as opposed to site–diagonal coupling which may lead to exciton self-trapping. Our choice was motivated by the fact that the Stokes shift in the emission spectra of many J aggregates is negligible.[7] In the localized excited state basis set $|n\rangle$, which denotes the state with a single excitation at site n, the exciton coherence operator $B_k^\dagger$ is given by

$$B_k^\dagger = \frac{1}{\sqrt{N}} \sum_{n=1}^{N} \exp\left(\frac{2\pi i k}{N} (n-1) \right) |n\rangle\langle 0|. \tag{2.3}$$

The state $|0\rangle$ is the ground state, in which all N molecules are unexcited. Note that H_e is not Hermitian because of the $\gamma(k)$ term; it is an effective Hamiltonian, derived from the complete matter–photon coupling Hamiltonian, and takes into account the radiative damping or superradiance of the k th exciton state. For a cyclic aggregate much smaller than an optical wavelength, we have[21]

$$\gamma(k) = N\gamma \delta_{k,0} \tag{2.4}$$

for the k-dependent radiation rate. Here γ is the spontaneous emission rate for an isolated monomer. Note that the $k = 0$ (totally symmetric) state decays N times faster than a single molecule and that the remaining states do not radiate, a phenomenon known as subradiance. The exciton energy $\omega(k)$ is given by

$$\omega(k) = \omega_0 - 2V \cos\left(\frac{2\pi k}{N} \right), \quad k = 0,1,\ldots,N-1, \tag{2.5}$$

where the dipole–dipole energy between molecules m and n, $-V_{mn}$, is

$$-V_{mn} = \frac{3\gamma}{4} \frac{(1 - 3\cos^2\theta_{12})}{(k_0 r_{mn})^3} \tag{2.6}$$

with $k_0 = \omega_0/c$, and $r_{mn} = |\mathbf{r}_m - \mathbf{r}_n|$ and $V \equiv V_{12}$ is the (negative of the) nearest-neighbor dipole–dipole coupling energy. In a J aggregate the absorption peak is red-shifted from the monomer peak; V is therefore a positive quantity, implying that $\cos^2\theta_{12} > 1/3$. In all our calculations we assume the J-aggregate configuration, although an equivalent analysis for an H aggregate ($V < 0$), where the optically selected exciton is at the top of the band, is simply performed by changing the sign of the V in the equations of motion.

The phonon Hamiltonian H_p gives the energy $\Omega_s(q)$ of the molecular vibrations when the system is in the electronic ground state. The subscript s refers to the phonon branch; a one-dimensional aggregate with one molecule per unit cell has a single acoustic phonon branch and a single optical phonon branch. The acoustic branch represents intermolecular vibrations and is characterized by an energy $\Omega_s(q)$ which vanishes as q approaches zero. The optical branch represents molecular librations and exhibits a nonzero value of $\Omega_s(q = 0)$. Each branch contains N modes characterized by the wave vector q. In Sec. V we will consider the effect of each of these types of phonons separately on the exciton fluorescence dynamics.

The exciton–phonon Hamiltonian describes exciton dephasing and population transfer due to the scattering off phonons. In this work, we explore the effect of the exciton–phonon Hamiltonian which arises from the (linear) change in the dipole coupling energy V when the molecules are dis-

placed or "twisted."[21] As is evident from Eq. (2.2c) the exciton number is conserved but the number of phonons is not. The coupling $F_s(k,q)$ for a one-dimensional aggregate is defined as[21]

$$F_s(k,q) = \sum_{m=1,-1} \sum_{l=1}^{2} e_s^l(q) \left[\frac{\hbar}{2I_l\Omega_s(q)}\right]^{1/2} \times \left\{\left[\frac{\partial}{\partial r_0^1} + \exp\left(\frac{2\pi iqm}{N}\right)\frac{\partial}{\partial r_m^l}\right] V_{0m}\right\}_0 \times \exp\left(\frac{2\pi ikm}{N}\right), \tag{2.7}$$

where $e_s^l(q)$ are the components of the unit polarization vectors of branch s, and l is the index for the general coordinate; $r_m^{l=1} \equiv r_m$ is the displacement of the mth molecule from its equilibrium value, and $r_m^{l=2} \equiv \theta_m$ is the angle which the mth transition dipole moment makes with the aggregate axis. I_l are the mass coefficients corresponding to the translational ($l=1$) or rotational ($l=2$) motion. The subscript "0" indicates that the derivatives are evaluated at the equilibrium configuration. Finally we note that since H_{ep} is Hermittian we have

$$F_s(k,q) = F_s^*(k+q, N-q).$$

III. REDUCED EQUATIONS OF MOTION

In this section we derive, starting with the Hamiltonian in Eq. (2.2), reduced equations of motion for the N exciton populations where the phonon variables have been eliminated. These equations allow us to calculate the time-resolved exciton fluorescence. We assume that at $t=0$ a short laser pulse coherently excites the $k=0$ aggregate exciton, and are interested in the subsequent exciton radiation in the presence of phonons. We should mention that higher exciton density effects such as exciton–exciton annihilation are not accounted for in our theory. These effects increase with the strength of the excitation source (the laser pulse energy for example) but are negligible in the weak excitation regime.

When a sample of M randomly oriented aggregates each consisting of N molecules is initially excited by a short pulse of area θ_p, the intensity of the incoherent fluorescence emitted in the unit direction $\mathbf{R}$ is given by[19]

$$I_{Fl}(\mathbf{R},t) = MN^2 s(\mathbf{R}) G(0,t), \tag{3.1}$$

where the direction factor $s(\mathbf{R})$ is

$$s(\mathbf{R}) = \frac{\theta_p^2}{4}\left[\frac{3\gamma}{8\pi}\right]\frac{4-2(\mathbf{R}\cdot\mathbf{x})^2}{15}. \tag{3.2}$$

Here, $G(k,t)$ is the normalized k th exciton population defined as

$$G(k,t) \equiv (4/N\theta_p^2)\langle B_k^\dagger(t) B_k(t)\rangle. \tag{3.3}$$

In Eq. (3.2), $\mathbf{x}$ is a unit polarization vector of the linearly polarized exciting laser pulse. Usually, one measures the radiation emitted at right angles to the laser pulse propagation axis $\mathbf{z}$, along the $\mathbf{R}=\mathbf{y}$ direction, in order to avoid detection of unwanted scattered laser light.

Immediately after laser pulse excitation, the exciton population is[19]

$$\langle B_k^\dagger(0) B_k(0)\rangle = \frac{N\theta_p^2}{4}\delta_{k,0}, \quad \theta_p \ll 1 \tag{3.4}$$

so that according to the definition Eq. (3.3),

$$G(k,0) = \delta_{k,0}. \tag{3.5}$$

In addition, all initial exciton coherences ($\langle B_k^\dagger(0) B_{k'}(0)\rangle (k \neq k')$ are zero. The laser pulse thus prepares the system in the $k=0$ exciton state. If we further assume that the transition dipole moment is independent of the nuclear coordinates, the initial phonon distribution is identical to the ground state thermal distribution.

In order to describe the subsequent exciton fluorescence in the presence of phonons, one needs to calculate the time dependent $k=0$ exciton population. To this end we use a procedure originally used by Bogolyubov and Tyablikov.[20] An infinite hierarchy of equations are derived by starting with the Heisenberg equation of motion for a material operator A_α, which has both exciton and phonon contributions:

$$\frac{d\langle A_\alpha(t)\rangle}{dt} = i\langle [H, A_\alpha]\rangle. \tag{3.6}$$

In our case we are interested in $A_\alpha = B_k^\dagger B_{k'}$, $B_k^\dagger B_{k'} b_q$, $B_k^\dagger B_{k'} b_q^\dagger$, $B_k^\dagger B_{k'} b_q^\dagger b_{q'}$, etc., all of which must be known as a function of time in order to calculate $B_0^\dagger(t) B_0(t)$ and hence the exciton fluorescence. Application of Eq. (3.6) for $A_\alpha = B_k^\dagger B_k$ produces an equation with terms like $\langle B_{k+q}^\dagger(t) B_k(t) b_q(t)\rangle$ and $\langle B_{k+q}^\dagger(t) B_k(t) b_q^\dagger(t)\rangle$ appearing on the right-hand side. A second application of Eq. (3.6) for $A_\alpha = B_{k+q}^\dagger(t) B_k(t) b_q(t)$ or $B_{k+q}^\dagger(t) B_k(t) b_q^\dagger(t)$ leads to an equation with source terms such as $\langle B_{k+q+q'}^\dagger(t) B_k(t) b_q^\dagger(t) b_{q'}(t)\rangle$, containing an additional phonon variable. Continuing in this fashion produces an infinite set of coupled equations, a hierarchy, where the ith level ($i=1,2,\ldots$) represents equations of motion for operator expectation values consisting of a product of the exciton k,k' coherence operator ($B_k^\dagger B_{k'}$) and $i-1$ phonon creation or annihilation operators. In order to reduce the number of equations to a manageable size, the expectation value of operators appearing in the source terms must be factorized, at some level i, into the product of the expectation value of exciton operator and the expectation value of phonon operators, thus forming a closed system of equations. In this work we apply this procedure to the second level in the hierarchy ($i=2$), performing the factorization on the source terms involved in the equations of motion for operator expectation values like $\langle B_{k+q}^\dagger(t) B_k(t) b_q(t)\rangle$. The factorization approximations are the following:

$$\langle B_{k+q+q'}^\dagger(t) B_k(t) b_{N-q}^\dagger(t) b_{q'}(t)\rangle \cong \langle B_k^\dagger(t) B_k(t)\rangle n_{q'}\delta_{N-q,q'}, \tag{3.7a}$$

$$\langle B_{k+q+q'}^\dagger(t) B_k(t) b_{N-q}(t) b_{q'}^\dagger(t)\rangle \cong \langle B_k^\dagger(t) B_k(t)\rangle (1+n_{q'})\delta_{N-q,q'}, \tag{3.7b}$$

$$\langle B_{k+q+q'}^\dagger(t) B_k(t) b_{N-q}^\dagger(t) b_{q'}^\dagger(t)\rangle = \langle B_k^\dagger(t) B_k(t) b_{N-q}(t) b_{q'}(t)\rangle \cong 0, \tag{3.7c}$$

where we have assumed, in addition, that the phonon field is unperturbed by the presence of excited state molecules, and remains in thermal equilibrium—an excellent approximation when the exciton density is low.[21] Here, n_q is the number of phonons of wave vector q and at temperature T, $n_q = \{\exp[\hbar\Omega(q)/kT] - 1\}^{-1}$.

The second level equations can now be formally integrated and substituted into the first level. This results in the following closed set of N coupled equations for the exciton populations, which constitutes a generalized master equation in k space:[22]

$$\frac{dG(k,t)}{dt} = -N\gamma\delta_{k,0}G(k,t) - \sum_q \int_0^t K_1(k,q;t-t')G(k,t') + \sum_q \int_0^t K_2(k,q;t-t')G(k+q,t'), \tag{3.8}$$

where the integral kernels K_1 and K_2 are given by

$$K_1(k,q;\tau) \equiv \frac{2}{N}|F(k,q)|^2\{(1+n_q)\cos[\Omega_+(k,q)\tau] + n_q\cos[\Omega_-(k,q)\tau]\}e^{-(N\gamma/2)[\delta_{k,0}+\delta_{k+q,0}]\tau}, \tag{3.9a}$$

$$K_2(k,q;\tau) \equiv \frac{2}{N}|F(k,q)|^2\{(1+n_q)\cos[\Omega_-(k,q)\tau] + n_q\cos[\Omega_+(k,q)\tau]\}e^{-(N\gamma/2)[\delta_{k,0}+\delta_{k+q,0}]\tau}, \tag{3.9b}$$

and the exciton–phonon frequency difference is defined as: $\Omega_\pm(k,q) = \omega(k+q) - \omega(k) \pm \Omega(q)$.

According to Eq. (3.8), population which is initially confined to the $k=0$ exciton state is redistributed over time among all other $N-1$ ($k \neq 0$) exciton populations due to the interaction with phonons. Simultaneously, the $k=0$ exciton population diminishes due to superradiant emission, represented by the first term on the r.h.s. in Eq. (3.8). Let us define the total excited state population as

$$P_T(t) \equiv \sum_{k=0}^{N-1} G(k,t).$$

Using Eq. (3.8) and the property $\Sigma_k\{-K_1(k,q,\tau) + K_2(k,q,\tau)\} = 0$ we get

$$\frac{d}{dt}P_T(t) = -N\gamma G(0,t). \tag{3.10}$$

The total excitonic population is affected only by superradiance. Phonon scattering does not affect the decay of the total exciton population, since H_{ep} conserves the total number of excitons. If we now introduce the nth temporal moment M_n of $dP_T(t)/dt$ as

$$M_n \equiv -\int_0^t t^n \dot{P}_T(t), \tag{3.11}$$

then by integrating Eq. (3.10) and using the initial condition Eq. (3.5) we get $M_0 = 1$, independent of phonon dephasing. The unitary value of M_0 along with Eqs. (3.1) and (3.5) show that the integrated fluorescence, representing the total number of emitted photons, is proportional to the aggregate size N and is independent of temperature or exciton–phonon coupling strength. Higher moments M_n ($n>0$) are affected by phonon scattering and reflect the change in the fluorescence decay profile, the calculation of which is the subject of this paper.

IV. THE TEMPERATURE-DEPENDENT COHERENCE SIZE

In this section we calculate the fluorescence decay [Eq. (3.1)] from aggregates as large as $N=400$ with exciton–phonon coupling, with particular attention given to the size and temperature dependence. This obviously requires a solution to Eq. (3.8) which is described in Appendix A. In Fig. 1, we show the fluorescence signal calculated by this procedure for an aggregate of size $N=20$ with exciton–acoustic phonon coupling. ($kT = 100\Omega_{ac}$, where Ω_{ac} is the acoustic phonon bandwidth [see Eq. (4.2)]). The rapid oscillations reflect the temporal memory of Eq. (3.8). In realistic samples these oscillations will be partially or completely washed by inhomogeneous broadening in the transition frequencies or a distribution of aggregate sizes. In addition, the finite temporal resolution of any experimental measurement of fluorescence may eliminate the fast oscillations. Under such circumstances, only the coarse-grained fluorescence decay is measured and this is the quantity of physical interest. The smooth solid curve in Fig. 1 shows the coarse-grained temporal response, calculated by convoluting a Gaussian function $D(\omega)$ with a width of $\sigma = 30N\gamma$, with the oscillating fluorescence decay (see Appendix A). As can be seen the coarse-grained response is in general nonexponential.

We have verified numerically that the timescale of the fast oscillations in the fluorescence decay is of the order of the polarization correlation time (T_2), which includes only the exciton–phonon scattering (and not the radiative com-

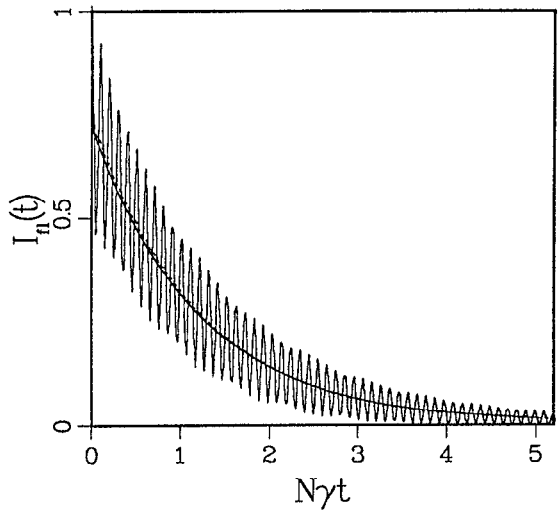

FIG. 1. The rapidly oscillating curve is the normalized fluorescence decay from an aggregate of size $N=20$ with acoustic phonons of frequency $\Omega_{ac} = 0.01V$, exciton–phonon coupling strength $F_{ac} = 0.01V$, and $kT = 100\Omega_{ac}$, calculated by numerically solving Eqs. (3.8) using Fourier transform techniques. The smooth, solid curve results from smoothing the oscillating curve by using a Gaussian filter function, $\exp[-(\omega/\sigma)^2]$ with $\sigma = 30N\gamma$. The dashed curve is the coarse-grained solution [Eq. (B5)].

ponent). By restricting the analysis to the regime $T_2 \ll (N\gamma)^{-1}$ it is then possible to derive the coarse-grained decay curve directly, under a time-local approximation, without first calculating the oscillating decay. The coarse-grained approximation (CGA) is described in Appendix B and results in an enormous saving in computer time. The dashed curve in Fig. 1 shows the decay calculated under the CGA. Note the excellent agreement with the smoothed "complete" solution (solid curve) which took roughly 1000 times more computer time.

We are now in a position to investigate the influence of optical and acoustic phonons on the radiative dynamics of a molecular aggregate. With one absorber per unit cell, N optical phonons correspond to the librational motion or twisting of the aggregate molecules about their equilibrium angle, θ_{12}. Acoustic phonons correspond to longitudinal vibrations along the aggregate axis, where a neighboring aggregate is displaced from its equilibrium nearest-neighbor distance. In all calculations we assume $T_2 \ll (N\gamma)^{-1}$ so that the CGA is justified. Even at zero temperature, this condition may hold when $F_{ac/op}$ is sufficiently large, because of exciton scattering off the zero-point phonon vibrations, or equivalently, because the $k=0$ exciton state is no longer an eigenstate of the aggregate and the oscillator strength is distributed over many $k \neq 0$ levels. To describe the situation where T_2 is of the order of $(N\gamma)^{-1}$ one must resort to the full numerical scheme to calculate the fluorescence. However, in the superradiant limit $T_2 \gg (N\gamma)^{-1}$, the aggregate radiates before the molecules have time to move, so that $G(0,t)$ is simply given by $\exp[-N\gamma t]$.

A. Acoustic phonons

The form of the exciton–phonon coupling depends on the phonon branch s and mode q. For an acoustic phonon branch we have the following coupling[21]

$$F_{ac}(k,q) = F_{ac}\cos\left[\frac{2\pi}{N}(k+q/2)\right]\sin\left(\frac{\pi}{N}q\right)\Big/\sqrt{\sin\left|\frac{\pi}{N}q\right|}, \tag{4.1}$$

where $F_{ac} = 3iV(\beta/r_{12})$ and $\beta^2 = \hbar(2I\Omega_{ac})^{-1}$ is the mean square amplitude of the zero point vibrations of a harmonic oscillator with mass I and frequency Ω_{ac}. For acoustic phonons the mode frequency is related to the wave vector via the dispersion relation:

$$\Omega_{ac}(q) = \Omega_{ac}\left|\sin\frac{\pi}{N}q\right|. \tag{4.2}$$

Because the fluorescence decay is generally multiexponential, there is an obvious ambiguity in the definition of the radiative decay rate. We have adapted the following operational definition: the radiative rate is the inverse of the time τ_{fl} it takes for the aggregate to emit $(1-e^{-1})$ of its initial energy. (τ_{fl} is defined through the equation $N\gamma\int_0^{\tau_{fl}} dt\, G(0,t) = 1 - 1/e$). In the superradiant limit, this is simply equal to $N\gamma$; when phonon interactions are important the rate is smaller and we can define an effective cooperation number $N_{eff}(N,T)$ to be the radiation rate as defined above divided by γ. The effective cooperation number satisfies $N_{eff} < N$ and is, in general, a function of aggregates size N, temperature T, exciton–photon coupling strength F_{ac}, phonon bandwidth Ω_{ac}, and exciton bandwidth $4V$.

In Fig. 2 we show N_{eff} vs N for aggregate with acoustic phonons (solid curves) for three values of the temperature, $kT/\Omega_{ac} = 1$, 10, and 100. The photon bandwidth is $\Omega_{ac} = 0.01V$ and the exciton phonon coupling is $F_{ac} = 0.01V$. N_{eff} is based on the fluorescence decay which is calculated numerically using the CGA. In the low temperature region, the aggregate behaves superradiantly and the decay rate increases linearly as a function of N. Here $N_{eff} = N$. At intermediate temperatures the decay rate levels off and remains constant as N increases. This allows the definition of a temperature-dependent cooperation number, $N^*(T)$, as the asymptotic limit of $N_{eff}(N,T)$ for large N. It represents the maximum coherence size attainable by an aggregate at a temperature T. (For brevity, the functional dependence of N^* on the other quantities is not indicated.) This statement is, of course, restricted to cases where the CGA is applicable, or $T_2 \ll (N\gamma)^{-1}$ which generally breaks down for very large N *as long as* the aggregate still remains much smaller than an optical wavelength. For infinite size aggregates (which extend far beyond an optical wavelength) with no phonons $N_{eff}(=N^*)$ is equal to (λ/a) in one dimension[17,23(a)] and $(\lambda/a)^2$ in two dimensions,[23(b)] and is not proportional to N as it is in the small aggregate limit. This fact modifies the inequality which justifies the CGA (see Sec. VI). The present work presents a microscopic calculation for the coherence size N^*, a quantity alluded to several times in the literature in phenomenological discussions of dephasing and radiative decay in semiconductor microstructures[10] as well as molecular aggregates.[6-8]

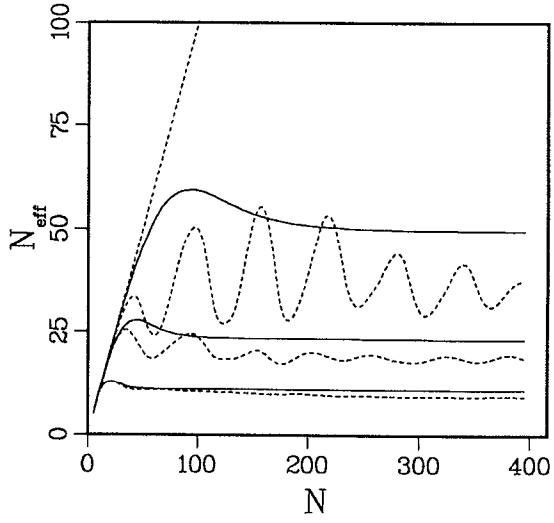

FIG. 2. The effective cooperation number N_{eff} as a function of aggregate size for acoustic phonons (solid curves) with $F_{ac} = 0.01V$ and $\Omega_{ac} = 0.01V$ and optical phonons (dashed curves) with the same parameters. Acoustic (optical) curves from top to bottom correspond to $kT/\Omega_{ac(op)} = 1$ (3.16), 10 (10), and 100 (100). The linear dashed curve is the superradiant limit, i.e., $N_{eff} = N$. The oscillations in the optical case are due to a resonance effect as discussed in the text.

As mentioned previously, the fluorescence decays are generally multiexponential. In Fig. 3 the normalized (natural log of the) fluorescence intensity is shown as a function of time for $N=100$ and for three temperatures ($kT/\Omega_{ac/op}=1$, 10, and 100). The solid (dashed) curves correspond to the acoustic (optical) phonon case. Note that as the temperature is increased the decays become slower; in the limit of very high temperature our numerical results recover the monomer decay rate (see Figs. 6, 7). We should point out that experiments by deBoer and Wiersma[7(a)] on PIC J aggregates show a single exponential fluorescence decay rate, which decreases as the temperature is increased.

Before considering a more general dependence of $N_{\rm eff}$ on all pertinent quantities, we first describe a resonant effect which results when the acoustic phonon frequency $\Omega_{ac}(q)$ closely matches the frequency difference between the kth exciton level and the $k=0$ exciton level, $\omega(k)-\omega(0)$, when the momentum selection rule $k=q$ is obeyed. In Fig. 4 we show $N_{\rm eff}$ vs N for the same parameters as in Fig. 2 except that $\Omega_{ac}/V=0.0622$. When $N=205$ and 410 there are pronounced dips, reflecting the condition

$$\Omega_{ac}(q=1)=k\,[\omega(1)-\omega(0)], \tag{4.3}$$

where the integer $k=1$ and 2 for the first and second dip, respectively. If we were to go out far enough we would observe resonant dips corresponding to all k. The condition is easily derived by equating $\Omega_{ac}(q)$ with $\omega(k)-\omega(0)$, for $q=k$, which in the limit that for $k\ll N$, becomes

$$\Omega_{ac}[\pi/N]\approx 4V[\pi^2 k/N^2],$$

which is the $N\gg 1$ limit of Eq. (4.3). From this last expression we obtain

$$N_{\rm res}\approx 4\pi V/\Omega_{ac}, \tag{4.4}$$

where $N_{\rm res}$ is the aggregate size at the first dip and is, of course, taken to be the nearest integer value of the r.h.s. of Eq. (4.4). The reason for a dip instead of a peak is that a resonant or nearly resonant phonon can more effectively couple two exciton levels leading to a more efficient population redistribution away from the initially excited $k=0$ state, and hence a reduced radiation rate, closer to that of the monomer. Note that the curves corresponding to $kT/\Omega_{ac}=10$ and 100 in Fig. 4 are, except for the dips, nearly the same as the corresponding curves in Fig. 2. (In Fig. 2 with $\Omega_{ac}=0.01V$, we get $N_{\rm res}=1200$.) This arises from a scaling relation which we will come to shortly. We therefore modify our definition of $N^*(T)$ so as to neglect the resonant regions of $N_{\rm eff}$ as a function of N. (Numerical results indicate that this region is much smaller than the plateau region for large $N_{\rm res}$. For small $N_{\rm res}$, $N_{\rm eff}$ is highly oscillating and $N^*(T)$ can be defined as the average $N_{\rm eff}$ in the large N limit.)

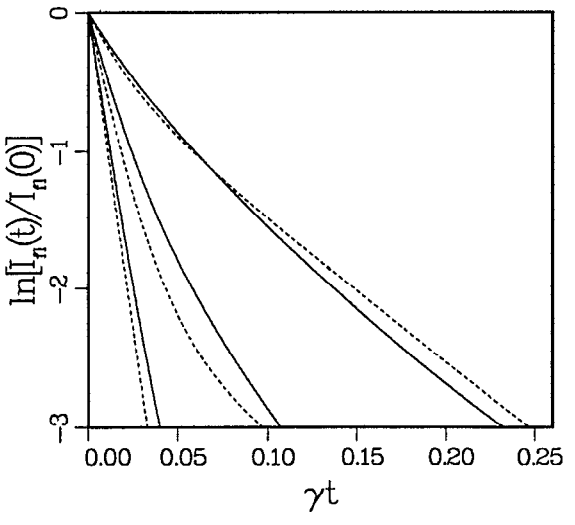

FIG. 3. The fluorescence decays for aggregates with acoustic (solid curves) and optical (dashed curves) exciton–phonon coupling with $F_{ac/op}=0.01V$, $\Omega_{ac/op}=0.01V$, and $N=100$. Fastest to slowest decays correspond to temperatures $kT/\Omega_{ac/op}=1$, 10, and 100. Note that at the lowest temperature the decays are close to superradiant.

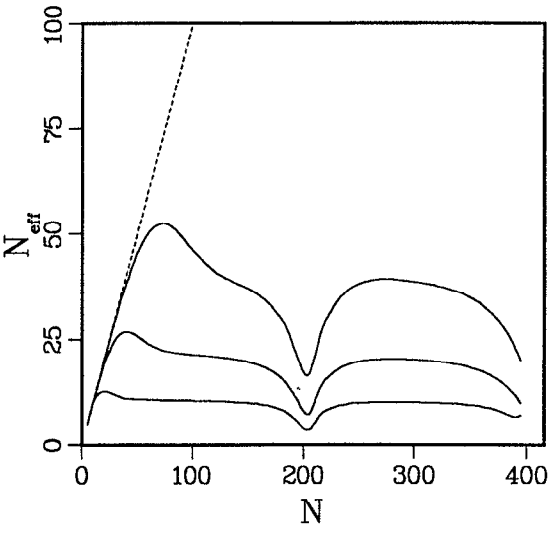

FIG. 4. The effective cooperation number $N_{\rm eff}$ as a function of aggregate size for acoustic phonons with $F_{ac}=0.01V$ and $\Omega_{ac}=4\pi V/205=0.0622V$, using the coarse-grained solution [Eq. (B5)]. The linear dashed curve is the superradiant limit, i.e., $N_{\rm eff}=N$.

In the course of our numerical investigation, we have found an important scaling relation for $N_{\rm eff}$ in the acoustic phonon case. Whenever $kT\gg\Omega_{ac}$ so that $n_q\approx kT/\Omega_{ac}$, and, in addition, when $N\neq\Delta N_{\rm res}$ (where $\Delta N_{\rm res}$ denotes the resonance region), $N_{\rm eff}$ depends on F_{ac}, Ω_{ac}, T, and V through the dimensionless parameter $\rho\equiv F_{ac}^2 kT/(V^2\Omega_{ac})$, i.e.,

$$N_{\rm eff}=N_{\rm eff}[N,\rho],\quad kT\gg\Omega_{ac},\quad N\neq\Delta N_{\rm res}. \tag{4.5}$$

The scaling ratio of parameters on the r.h.s. of Eq. (4.5) also appear in Eq. (A2) as the prefactor to the $T^{(\pm)}(s{:}k,q)$ function, which contains the resonance behavior. In Fig. 5 we plot $\log_{10}[F_{ac}^2/V^2]$ vs $\log_{10}[\Omega_{ac}/V]$ for $kT/V=1$, 10, and 100. The curves were obtained by numerically searching for the value of F_{ac}/V, given Ω_{ac}/V, kT/V, and $N=100$, which gives $N_{\rm eff}=10$. The curves are therefore contour curves of constant $N_{\rm eff}$. They clearly show that for a given temperature, $N_{\rm eff}=10$, when the ratio $F_{ac}^2/(\Omega_{ac}V)$ is constant. (This is evident because the slope of the log–log plot is equal to unity). In addition, an increase in temperature by a factor of 10 simply results in a downward vertical translation

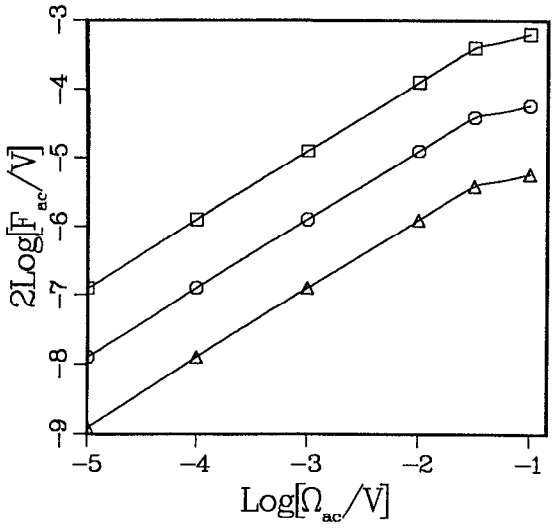

FIG. 5. All points on the curves correspond to $N_{\rm eff} = 10$. The three curves correspond to $kT/V = 1$, 10, and 100 from top to bottom. $N = 100$ in all calculations while $F_{\rm ac}$ which gives $N_{\rm eff} = 10$ was searched numerically.

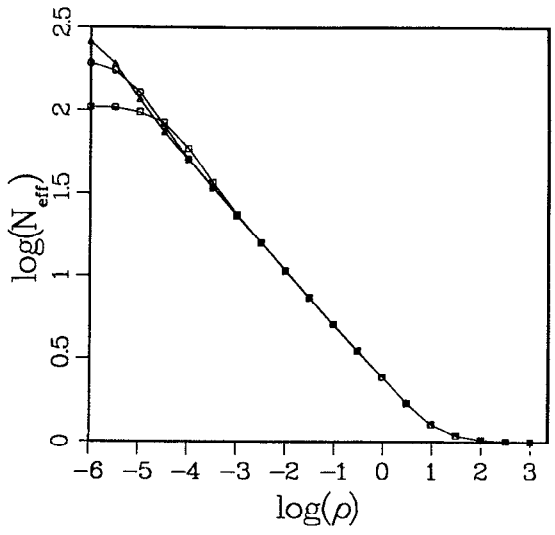

FIG. 6. $\log[N_{eff}]$ vs $\log[\rho]$, where $\rho = (F_{\rm ac}^2/V^2)kT/\Omega_{\rm ac}$. For all points $\Omega_{\rm ac} = 0.01V$ and $F_{\rm ac} = 0.01$ V and the temperature is varied. When $kT/\Omega_{\rm ac} \gg 1$, the scaling relation Eq. (4.6) is valid. The three curves correspond to $N = 105$ (bottom), 205 (middle), and 305 (top). When the $N = 205$ and $N = 305$ curve coincide $N_{\rm eff} = N^*$. Note the activated temperature dependence for N_{eff} is more pronounced for smaller size aggregates (because of the more discrete phonon band structure) and disappears for larger N. The slope of the linear portion is approximately $-1/3$.

of exactly one unit, meaning that the ratio $[F_{\rm ac}^2/V^2][kT/V]$ is constant for $N_{\rm eff} = 10$. The deviation from linearity for $\Omega_{\rm ac} \simeq 0.01V$ occurs because N is approaching the resonance region, where the scaling law is no longer valid.

With the scaling law in hand we now investigate the functional dependence of N^* on ρ. In Fig. 6, $\log_{10}[N_{\rm eff}]$ is plotted against $\log_{10}(\rho)$ when $F_{\rm ac} = 0.01V$ for $N = 100$, 200, and 300. N^* is equal to $N_{\rm eff}$ when $N_{\rm eff}$ has converged, in this case when the curves for $N = 200$ and $N = 300$ coincide, which is when $kT/\Omega_{\rm ac}$ is greater than approximately one. In this range, we therefore can view the graph as N^* vs $kT/\Omega_{\rm ac}$. Also when $kT/\Omega_{\rm ac} > 10$ we are in a region where the scaling law is valid. ($\Omega_{\rm ac}$ was held fixed at $0.01V$, while the temperature was varied, giving $N_{\rm res} = 1200$ and therefore in all cases $N \neq \Delta N_{\rm res}$.) We find, rather remarkably, that in this region the log–log plot is linear to an excellent approximation, with a slope of -0.325. We thus have the empirical relation:

$$N^*(\rho) \cong 2.16\rho^{-1/3}, \quad 10^5 > kT/\Omega_{\rm ac} \gg 1, \quad N \neq \Delta N_{\rm res}. \tag{4.6}$$

Note also from Fig. 6 that in the limit of very high temperatures, $N_{\rm eff}$ approaches one, the monomer value.

B. Optical phonons

For an optical phonon, where only the nearest-neighbor dipole–dipole coupling is retained, the coupling with excitons takes the form:[21]

$$F(k,q) = F_{\rm op} \cos\left[\frac{2\pi}{N}(k + q/2)\right]\cos\left(\frac{\pi}{N}q\right) \tag{4.7}$$

with $F_{\rm op} = 3\eta V(\sin 2\theta_{12}/(1 - 3\cos^2\theta_{12}))$ and $\eta^2 \equiv \hbar(2I\Omega_{\rm op})^{-1}$ is the mean square displacement of the zero-point angular vibrations at frequency $\Omega_{\rm op}$. For a dispersionless optical phonon, the mode frequency does not depend on the wave vector:

$$\Omega_{\rm op}(q) = \Omega_{\rm op}. \tag{4.8}$$

The dashed curves in Fig. 2(b) correspond to $N_{\rm eff}$ vs N for an aggregate with a dispersionless optical phonon at $kT/\Omega_{\rm op} = 3.16$, 10, and 100 with $\Omega_{\rm op} = 0.01V$ and $F_{\rm op} = 0.01V$. As with the acoustic phonon case, $N_{\rm eff}$ initially increases linearly with aggregate size. This is the superradiant regime, where $N_{\rm eff} = N$. Further increases in N result in an oscillation of $N_{\rm eff}$ about a stable value, which we define as $N^*(T)$. The oscillations are due to resonant exciton–phonon coupling, and the k th resonant dip roughly corresponds to the condition $\omega(k) - \omega(0) = \Omega_{\rm op}$, i.e., when the phonon frequency is in resonance with the difference between the k th exciton and the $k = 0$ exciton. The values of N corresponding to this condition are

$$N_{\rm nes} = 2\pi\sqrt{V/\Omega_{\rm op}}\,k \tag{4.9}$$

when $k \ll N$. (Again, we take the closest integer value for $N_{\rm res}$.) Thus, the various dips appear at regular intervals. [When $N_{\rm eff}$ is based on the $1/e$ fluorescence time, the oscillations appear exactly as predicted by Eq. (4.10).] This resonance behavior is clearly seen in Fig. 2, and is qualitatively different from the acoustic phonon case. For equal values of $\Omega_{\rm ac}$ and $\Omega_{\rm op}$, comparison of Eq. (4.4) and Eq. (4.9) shows that the resonances occur much earlier in the optical phonon case. (When $\Omega_{\rm ac} = \Omega_{\rm op} = 0.01V$, we have $N_{\rm res} = 1200$ and $N_{\rm res} = 63$ for the acoustic and optical cases, respectively.) Also, the optical phonon resonances appear to vanish for sufficiently high temperature (making the definition of N^* straightforward) while the acoustic phonon resonances persist.

We have investigated a possible scaling relation for optical phonons and have found that as long as $kT \gg \Omega_{\rm op}$ and

$\Omega_{op} < 0.01V$, N_{eff} depends on the same scaled variable as the acoustic phonon case. In Fig. 7 we show $\log_{10}[N_{eff}]$ vs $\log_{10}(\rho)$ for $N = 100$, 200, and 300. (Ω_{op} was held at $10^{-3}V$ while the temperature was increased, so that the scaling relation is valid for high temperatures.) The $N = 200$ and $N = 300$ curves coincide for $kT/\Omega_{op} > 1$, so that in this region $N_{eff} = N^*$. Unlike the acoustic case, the log–log plot does not yield a linear relationship. One can appreciate an activated temperature dependence, where the effect of the optical phonon on the radiative decay rate is not "felt" until some threshold temperature, $kT_c \approx 0.2\Omega_{op}$ which is essentially size independent for large N. This is due to the exponentially activated dependence of the phonon number on the temperature, and the fact that the exciton–phonon coupling is proportional to this number. Beyond the threshold temperature, however, Figs. 4 and 6 overlap completely in the region from $kT/\Omega_{op} = 10$ to about 1000, so that in this region one can use the $T^{-1/3}$ power law [Eq. (4.6)] to describe the effect of optical phonons on the aggregate radiative decay rate. Beyond the scaling regime, the $T^{-1/3}$ relation breaks down.

V. COMPARISON WITH STRONG COLLISION MODELS

The present microscopic model of exciton–phonon coupling requires a numerical solution of the reduced equations of motion [Eq. (3.8)]. A qualitative picture of the quenching of superradiance can be obtained by considering a simplified but exactly soluble relaxation model.[24,25] This can be obtained by making the following approximations to Eq. (3.8):

(1) We assume that the relaxation kernels have a short correlation time (Markovian limit) so that the temporal dependence of K_1 and K_2 can be approximated by delta functions. Equation (3.8) then reduces to an ordinary master equation.

(2) We simplify the kernels by assuming a strong collision (BGK) model where K_1 and K_2 are taken to be independent of q. We thus obtain the following master equation:

$$\frac{dG(k,t)}{dt} = -N\gamma\delta_{k,0}G(k,t) + \Gamma\sum_{k'}[f(k)G(k',t) - f(k')G(k,t)]. \tag{5.1}$$

Here Γ is a scattering rate and $f(k)$ is a given equilibrium distribution of k states, with $\Sigma_{k=0}^{N-1} f(k) = 1$. When $\gamma = 0$, $G(k,t)$ will relax at long times to $f(k)$. The Haken–Strobl mode,[17] which assumes that the transition frequency of each molecule is undergoing independent and rapid, delta function correlated fluctuations of magnitude Γ, is a special case of the present strong collision model[25] with $f(k) = 1/N$. The fluorescence decay can be calculated analytically from Eq. (5.1) resulting in

$$G(0,t) = \frac{\Gamma f(0)(\gamma^+ - \Gamma)}{(\gamma^+ - N\gamma - \Gamma)(\gamma^- - \gamma^+)}\exp[-\gamma^+ t] + \frac{\Gamma f(0)(\gamma^- - \Gamma)}{(\gamma^- - N\gamma - \Gamma)(\gamma^+ - \gamma^-)}\exp[-\gamma^- t], \tag{5.2}$$

where $\gamma^{\pm}$ are given by

$$\gamma^{\pm} = \frac{N\gamma + \Gamma}{2} \pm \frac{1}{2}\sqrt{(\Gamma + N\gamma)^2 - 4Nf(0)\gamma\Gamma}\,. \tag{5.3}$$

Equation (5.2) has the following limiting behavior:

$$G(0,t) = \begin{cases} \exp(-N\gamma t), & \Gamma \ll N\gamma \quad (5.4a) \\ [1 - f(0)]e^{-\Gamma t} + f(0)e^{-f(0)N\gamma t}, & \Gamma \gg N\gamma. \quad (5.4b) \end{cases}$$

Equation (5.4a) shows that the fluorescence decay given by Eq. (5.2) agrees with the solution of Eq. (3.8) in the superradiant limit $\Gamma \ll N\gamma$. In the fast dephasing limit [Eq. (5.4b)] the decay is biexponential. The timescale of the fast part of the decay [first term in Eq. (5.4b)] corresponds to the polarization correlation time (T_2) which can be averaged away as we have done under the CGA (a negligible amount of photons are radiated during Γ^{-1}). The resulting decay is then a single exponential decay with decay rate equal to $f(0)N\gamma$, a result which agrees with Ref. 26. The temperature dependence is qualitatively similar to that obtained through the solution of Eq. (3.8); as the temperature increases $f(0)$ decreases and the lifetime therefore increases. However, Eq. (5.4b) does not show a size-independent coherence length N^*.

The quenching of superradiance induced by the Haken–Strobl model was studied in Ref. 17, where the first moment of the fluorescence decay or M_1 and its variations with the dephasing rate were calculated. (M_1 was denoted S^{-1} in Ref. 17). Figure 8 of Ref. 17 shows that this first moment is highly sensitive to small ($\Gamma \ll \gamma$) values of Γ. This sensitivity is due to the second term in Eq. (5.2). If we calculate the first moment (M_1) in the superradiant regime ($\Gamma \ll N\gamma$) using

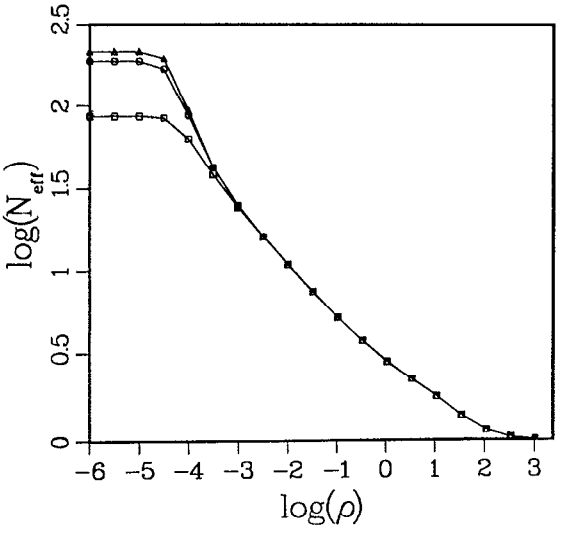

FIG. 7. $\log[N_{eff}]$ vs $\log[\rho]$, where $\rho = (F_{op}^2/V^2)kT/\Omega_{op}$. For all points $\Omega_{op} = 0.001V$ and $F_{ac} = 0.01V$ and the temperature is varied. For $kT/\Omega_{ac} \gg 1$, the scaling relation Eq. (4.6) is valid. The three curves correspond to $N = 105$ (bottom), 205 (middle), and 305 (top). When the $N = 205$ and $N = 305$ curves coincide $N_{eff} = N^*$. Note the activated temperature dependence for N_{eff} persists for all sizes N. In the range from $\rho = -3$ to $\rho = 0$ has a slope of approximately $-1/3$.

Eq. (5.2) with $f(0) = 1/N$ and Eq. (3.11) we get $M_1 = (N\gamma)^{-1} + (1 - 1/N)\gamma^{-1}$, where the first term originates from the first term in Eq. (5.2) and likewise for the second term. This calculation implies that in the superradiant regime and for $N \gg 1$ the average emission time is γ^{-1} which reflects a monomer decay rate. This arises because the second term in Eq. (5.2) has a coefficient of order Γ^2 and a subradiant decay rate of order Γ/N. It has practically no amplitude but decays so slowly that its first moment can be very large, and in fact exceeds the superradiant average lifetime $(N\gamma)^{-1}$ by a factor of N. In Ref. 17 it is shown that the second term actually contains a factor like $\Gamma^2/(\Gamma^2 + O[\gamma(kNa)^2]$ where Na is the aggregate length and k is the optical wave vector. This term now vanishes as Γ goes to zero; however, when Γ is of the order of $O[\gamma(kNa)^2]$, the second term attains a value close to γ^{-1}. This explains the high sensitivity of S^{-1} to Γ when kNa is very small (in our work with small aggregates we assume this quantity is zero). Therefore, the first momentum (M_1) does not provide a useful measure for the characteristic decay time. This is what motivated us to define the characteristic decay time, τ_{fl} to be the time at which $1 - 1/e$ of the total number of photons have been emitted. With this definition the second term in Eq. (5.2) would not contribute at all to τ_{fl}.

VI. CONCLUSION

We have theoretically investigated the radiation dynamics of molecular aggregates at finite temperature and have established the existence of a coherence size N^*, which determines the cooperative radiative dynamics of the entire aggregate of size N, where $N > N^*$. N^* is a result of the competition between exciton–phonon scattering and superradiance and is calculated microscopically, based on a reduced equation of motion for the N exciton populations. A coarse-grained approximation, in which rapid oscillations in the fluorescence decay are smoothed out was employed in order to simplify the numerics. Experimentally this is equivalent to a nonzero instrumental response time, since only the low frequency components of the fluorescence decay survive. The approximation works best at sufficiently high temperatures or exciton–phonon coupling strengths, such that the dephasing time is much shorter than the superradiant decay time, $T_2 \ll (N\gamma)^{-1}$. The oscillations are then extremely fast on the timescale of the overall radiative decay and can easily be averaged away without affecting longer timescale dynamics.

We have verified numerically that for large values of N the *entire* (normalized) fluorescence decay (not just N_{eff}) is independent on N. Since N^* is derived under the coarse-grained approximation it is restricted to aggregates sizes which obey $T_2 \ll (N\gamma)^{-1}$, which puts an upper bound on the (small) aggregate size N at a given temperature T, above which our results are not applicable. Let us denote this upper bound as $N_u \equiv (T_2\gamma)^{-1}$. We expect that the plateau behavior as seen in Fig. 2 (which defines N^*) will no longer hold when $N \approx N_u$. Certainly, when $N \gg N_u$ the small aggregate will superradiate before any nuclear motion can occur, and therefore the linear behavior $N_{\text{eff}} = N$ will be recovered for very large aggregates.

Time-resolved measurements such as fluorescence and absorption recovery in J aggregates[6,7,27–30] provide evidence for exciton superradiance, i.e., an enhanced radiative decay rate which scales linearly with the aggregate size. We should point out that most fluorescence lifetime measurements[29,30] for PIC aggregates vary greatly—from several picoseconds to about 1 ns—because the typically high excitation pulse energies used in each experiment caused the lifetime to be dominated by nonlinear exciton–excition annihilation. In the low intensity experiments in Ref. 7, exciton–exciton annihilation is absent and the decay reflects only superradiant dynamics. The recent work of DeBoer and Wiersma, showed that aggregates of pseudo-isocyanine bromide (PIC-Br) radiate 50–100 times faster than the monomer at low temperature (1.5 K), with a quantum yield close to unity.[7] Evidence of superradiant decay rates in J aggregates in solution and on surfaces was also given by Dorn and Muller.[27] Photon echo experiments by Wiersma *et al.*[7(b)] have shown that T_2 for PIC Br is approximately 10 ps (about an order of magnitude shorter than the superradiant fluorescence lifetime) measured at 1.5 K. Using $\gamma^{-1} = 3.7$ ns gives $N_u = 370$ at 1.5 K. For higher temperatures, however, T_2 decreases; at 100 K $T_2 \approx 1$ ps and N_u is increased to 3700.

The arguments just presented apply only for a small aggregate ($Na \ll \lambda$), with superradiative decay rate equal to $N\gamma$. For extended samples with dimensions much greater than an optical wavelength the superradiative decay rate no longer increases linearly with N but converges to roughly $(\lambda/a)\gamma$ [Ref. 23(a)] for a one-dimensional aggregate, and $(\lambda/a)^2\gamma$ (Ref. 29) for a two-dimensional monolayer. Therefore, our results are strictly valid for $N \ll \lambda/a$. Even so, we postulate that N^* ($\ll N_u$) derived numerically, can be valid for any size aggregate. Our reasoning is as follows. We know that N^* for the *small* aggregate is valid as long as $N \ll N_u$. Now, since the maximum superradiation rate for any size aggregate is $(\lambda/a)\gamma$ and not $N\gamma$, then our results, which depend on the coarse grained approximation, are valid when $T_2 \ll [(\lambda/a)\gamma]^{-1}$ is satisfied, which is *always* true if $N_u \gg \lambda/a$. In other words, the maximum superradiation rate can never reach the value $N_u\gamma$ if this requires the sample to extend beyond an optical wavelength, and therefore, at sufficiently high temperature, pure phonon dephasing can dominate for any size aggregate. Now, when $T_2(T) \ll [(\lambda/a)\gamma]^{-1}$, we postulate that extended geometry effects can be ignored as long as $N^*a \ll \lambda$, and $N^*\gamma$ is the convergent radiative rate for any size aggregate. This seems likely because extended geometry effects are not felt over the correlation distance N^*a. For PIC Br, we have $a \approx 10$ Å, $\lambda \approx 6000$ Å, and $\gamma \approx (3.7 \text{ ns})^{-1}$. Therefore $T_2(1.5 \text{ K}) = 10$ ps does not satisfy $T_2(T) \ll [(\lambda/a)\gamma]^{-1}$ and $N^*(1.5 \text{ K})\gamma$ would probably not represent the convergent decay rate for an infinitely long aggregate. However, at 100 K the inequality is satisfied and as long as $N^* \ll 600$, $N^*(100 \text{ K})\gamma$ should represent the convergent decay rate for an infinitely long aggregate. We are currently investigating extended geometry effects in greater detail, in order to prove our assertion.

Finally some comments regarding the temperature dependence of N^* are in order. We have shown theoretically that when low frequency optical or acoustic phonons are

responsible for the disruption of superradiance (in the scaling regime), $N^* \sim T^{-1/3}$ over several orders of magnitude in $kT/\Omega_{ac/op}$. However, when outside the scaling regime, i.e., $\Omega_{ac} > 0.1$ V or $\Omega_{op} > 0.01$ V, the temperature dependence can be quite different. deBoer and Wiersma[7(a)] have measured an activated temperature dependence for N_{eff} for PIC Br aggregates in a glass matrix, whereby $N_{eff} \sim T^{-1}$ above a threshold temperature of 50 K. As mentioned earlier, we have managed to fit this dependence with a relatively high frequency optical phonon $\Omega_{op} = 240\ cm^{-1}$ using our one-dimensional model,[31] so that a linear temperature dependence is also consistent with our model. In addition Mobius and Kuhn,[6] by different methods (based on energy transfer rates instead of fluorescence lifetimes), have determined an experimental cooperation length with the dependence $N^* = 3000/T$ for a J-aggregate monolayer.

ACKNOWLEDGMENTS

We wish to thank Professor D. Wiersma, Dr. A. Muenter, and Dr. D. Brumbaugh for useful discussions. The support of the National Science Foundation, the Air Force Office of Scientific Research, and the Petroleum Research Fund sponsored by the American Chemical Society is gratefully acknowledged. We also wish to thank the support of the Center for Photoinduced Charge Transfer sponsored by the National Science Foundation, and a generous grant of supercomputing time from CRAY Corporation, which made this work possible.

APPENDIX A: NUMERICAL SOLUTION OF EQ. (3.8)

Equation (3.8) is an integro-differential equation in time. The time derivative of the k th exciton population at time t depends on the temporal history of all exciton populations. We have developed numerical schemes to solve Eq. (3.8) and have obtained the radiative decay for aggregates as large as $N = 400$. It proves convenient for computational purposes to solve Eq. (3.8) in the Laplace domain. A Laplace transform on Eq. (3.8) leads to

$$s\tilde{\mathbf{G}}(s) - \mathbf{G}(0) = \mathbb{M}(s)\tilde{\mathbf{G}}(s), \tag{A1}$$

where we have introduced a vector–matrix notation for simplification. Here, the k th exciton population is denoted $[\mathbf{G}(t)]_k = G(k,t)$ and the Laplace transform of $G(k,t)$ is represented as $[\tilde{\mathbf{G}}(s)]_k \equiv \tilde{\mathbf{G}}(k,s)$. The coupling is contained in the matrix $\mathbb{M}(s)$:

$$[\mathbb{M}(s)]_{kk'} = \left[-N\gamma\delta_{k,0} - \frac{2}{N}\sum_{q\neq 0} |F(k,q)|^2\{(1+n_q)T^+(s;k,q) + n_q T^-(s;k,q)\}\right]\delta_{kk'}$$
$$+ \left[\frac{2}{N}|F(k,k'-k)|^2\{(1+n_{k'-k})T^-(s;k,k'-k) + n_{k'-k}T^+(s;k,k'-k)\}\right](1-\delta_{k,k'}), \tag{A2}$$

where $T^{(\pm)}(s;k,q)$ is defined as

$$T^{(\pm)}(s;k,q) \equiv \frac{s + (N\gamma/2)[\delta_{k,0} + \delta_{k+q,0}]}{\{s + (N\gamma/2)[\delta_{k,0} + \delta_{k+q,0}]\}^2 + \Omega_{\pm}(k,q)^2} \tag{A3}$$

and it follows from the definition of $\Omega_{\pm}(k,q)$ and Eq. (A3) that $T^+(k,q) = T^-(k+q,N-q)$.

The numerical procedure consists of evaluating the Fourier transform of $G(k,t)$, which is equal to $\tilde{G}(k,s=i\omega)$, for several thousand values of ω, and performing a fast Fourier transform back into the time domain. Numerical convergence was improved by calculating the symmetric function $G_s(k=0,t) = \theta(t)G(k=0,t) + \theta(-t)G(k=0,-t)$. It can be immediately shown that the respective Fourier transforms obey $\tilde{G}_s(k=0,i\omega) = 2\,\mathrm{Re}[\tilde{G}(k=0,i\omega)]$. The (inverse) fast Fourier transform of $\tilde{G}_s(k=0,i\omega)$ converges faster than a similar operation on $\tilde{G}(k=0,i\omega)$. In addition, we also performed calculations implementing a smoothing procedure by multiplying the symmetric function $\tilde{G}_s(k=0,i\omega)$ with, for example, a Gaussian function of the form $D(\omega) = \exp[-(\omega/\sigma)^2]$ and transforming back to the time domain via the FFT.

APPENDIX B: COARSE-GRAINED SOLUTION OF EQ. (3.8) (THE CGA)

We show in this appendix that in order to obtain the coarse-grained fluorescence decay it is not necessary to first calculate the complete rapidly oscillating response by the method of Appendix A and then perform a smoothing. When the polarization correlation time T_2 satisfies $T_2 \ll (N\gamma)^{-1}$ the coarse-grained decay curve can be calculated directly without first having to calculate the Fourier transform $\tilde{G}(k,i\omega)$. We define the coarse-grained response $\mathbf{g}(t)$ as the inverse Laplace transform of

$$\tilde{\mathbf{g}}(s) \equiv D(s)\tilde{\mathbf{G}}(s) = D(s)\frac{\mathbf{G}(0)}{s - \mathbb{M}(s)} \tag{B1}$$

where $D(s)$ is a frequency filter function with $D(0) = 1$. If we adjust the bandwidth of $D(s)$ to be much larger than the low frequency components of $\tilde{\mathbf{G}}(s)$ but much smaller than the high frequency components, then we can efficiently separate these two behaviors. This coarse-grained approximation (CGA) is justified when $1/T_2 \gg \text{bandwidth}(D) \gg N\gamma$, and is therefore better satisfied at higher temperatures or for larger exciton–phonon coupling strengths. The low frequency part of $\tilde{\mathbf{G}}(s)$ is obtained by including poles in Eq. (4.4) arising only from small values of s. These are found by using the first order (in s) approximation of $\mathbb{M}(s)$ in Eq. (4.4), obtained by expanding the coupling matrix $\mathbb{M}(s)$ in a Taylor series about $s = 0$.

$$\mathbb{M}(s) = \mathbb{M}_0 + \mathbb{M}_1 s + \cdots, \tag{B2}$$

where $\mathbb{M}_0 \equiv \mathbb{M}(0)$, and the matrix $\mathbb{M}_1 \equiv [\partial\mathbb{M}(s)/\partial s]|_{s=0}$ is obtained by replacing $T^{\pm}(s;k,q)$ in Eq. (A2) by $t_1^{\pm}(k,q) \equiv \partial T^{\pm}(s;k,q)/\partial s$ and omitting the first (superra-

diant) term. $t_1^{\pm}(k,q)$ is

$$t_1^{\pm}(k,q) = \frac{\Omega_{\pm}(k,q)^2 - [(N\gamma/2)(\delta_{k+q,0} + \delta_{k,0})]^2}{[[(N\gamma/2)(\delta_{k+q,0} + \delta_{k,0})]^2 + \Omega_{\pm}(k,q)^2]^2}. \tag{B3}$$

Within this first order approximation, Eq. (A1) becomes

$$s\tilde{\mathbf{N}}\tilde{\mathbf{g}}(s) - \mathbb{M}_0\tilde{\mathbf{g}}(s) = \mathbf{G}(0), \tag{B4}$$

where $\mathbf{N} = \mathbb{1} - \mathbb{M}_1$ and $\mathbb{1}$ is the identity matrix. By multiplying both sides by $\mathbf{N}^{-1}$, and diagonalizing $\mathbb{P} \equiv -\mathbf{N}^{-1}\mathbb{M}_0$ via $\mathbf{P}(\text{diag}) = \mathbb{U}^{-1}\mathbb{P}\mathbb{U}$ (the columns of $\mathbb{U}$ are the eigenvectors of $\mathbb{P}$), we can write the solution to Eq. (B4) as

$$[\tilde{\mathbf{g}}(s)]_k = \sum_{j=1}^{N} \frac{w_{k,j}}{s + p_{jj}}, \tag{B5}$$

where $w_{k,j} = [\mathbb{U}]_{kj}[(\mathbf{N}\mathbb{U})^{-1}\mathbf{G}(0)]_j$. The time domain fluorescence decay ($k = 0$) from Eq. (B5) is simply the sum of N exponentials each with time constant $1/p_{jj}$ and weight $w_{0,j}$. In Fig. 1 the dashed line corresponds to this solution. As is evident, it agrees very well with the smoothed solid fluorescence decay.

The coarse-grained solution retains all of the essential physical properties of the full solution. If we define the coarse-grained total exciton population as

$$p_T(t) \equiv \sum_{k=0}^{N-1} [\mathbf{g}(t)]_k,$$

then the analogous equation to Eq. (3.11) holds for the coarse-grained solution as well:

$$\frac{d}{dt}p_T(t) = -N\gamma[\mathbf{g}(t)]_{k=0}. \tag{B6}$$

If we define the corresponding temporal moments as $m_n \equiv -\int_0^t t^n \dot{p}_T(t)$, then it is easy to show that

$$m_0 = M_0 = 1 \tag{B7}$$

and

$$m_1 = M_1. \tag{B8}$$

These relations follow from the fact that the nth temporal moment of a function $F(t)$ is equal to $-i^n d^n F(\omega)/d\omega^n$ in Fourier space and the fact that $\tilde{\mathbf{g}}(s)$ and $\tilde{\mathbf{G}}(s)$ agree to first order in $s = i\omega$. Equation (B7) shows the quantum yield in the coarse-grained approximation remains independent of temperature and exciton–phonon coupling, while Eq. (B8) shows that the average or mean time of the decay is also identical. One property that is not common to both $\mathbf{g}(t)$ and $\mathbf{G}(t)$ is the initial condition. In the coarse-grained solution $[\tilde{\mathbf{g}}(t=0)]_{k=0}$ is not equal to unity as is $[\tilde{\mathbf{G}}(t=0)]_{k=0}$. This is a necessary feature of the averaging process; in the smoothed (solid line) decay of Fig. 1 the signal does not start at unity either. However, in the coarse-grained approximation the sum of the (normalized) exciton populations, $p_T(0)$ is still equal to unity at $t = 0$; a property which follows directly from Eqs. (B6) and (B7).

The numerical evaluation of $[\mathbf{g}(t=0)]_{k=0}$ is considerably faster than $[\mathbf{G}(t=0)]_{k=0}$. This is because only a few matrix manipulations are required to obtain the entire signal in the former case, while thousands of matrix manipulations are required to obtain the signal in the latter case (one matrix manipulation for each point). This saving of 10^3–10^4 in computer time also allows the investigation of much larger aggregate sizes. For example, with the Cray supercomputer an aggregate size of $N = 60$ takes about 15 min for a $[\mathbf{G}(t=0)]_{k=0}$ calculation (using 8192 values of s), whereas less than a second to calculate $[\mathbf{g}(t=0)]_{k=0}$, making a low frequency response calculation for $N \sim 10^3$ entirely feasible.

[1] P. B. Gilman, Phot. Sci. Eng. **18**, 418 (1974).
[2] G. Feher and M. Y. Okamura, in *The Photosynthetic Bacteria*, edited by R. K. Clayton and W. F. Sistrom (Plenum, New York, 1978).
[3] E. Hanamura, Phys. Rev. B **37**, 1273 (1988).
[4] F. C. Spano and S. Mukamel, Phys. Rev. A **40**, 5783 (1989).
[5] H. Ishihara and K. Cho, Phys Rev. B **42**, 1724 (1990).
[6] (a) D. Mobius and H. Kuhn, Israel J. Chem. **18**, 375 (1979); (b) D. Mobius and H. Kuhn, J. Appl. Phys. **64**, 5138 (1988).
[7] (a) S. DeBoer and D. A. Wiersma, Chem. Phys. Lett. **165**, 45 (1990); (b) S. DeBoer, K. J. Vink, and D. A. Wiersma, *ibid.* **137**, 99 (1987).
[8] Y. R. Kim, M. Lee, J. R. G. Thorne, R. M. Hochstrasser, and J. M. Ziegler, Chem. Phys. Lett. **145**, 75 (1988).
[9] T. Itoh, T. Ikehara, and Y. Iwabuchi, J. Lumin. **45**, 29 (1990).
[10] J. Feldmann, G. Peter, E. O. Gobel, P. Dawson, K. Moore, C. Foxon, and R. J. Elliot, Phys. Rev. Lett. **59**, 2337 (1987).
[11] F. Minami, A. Hasegawa, S. Asaka, and K. Inoue, J. Lumin. **45**, 409 (1990).
[12] E. W. Knapp, Chem. Phys. **85**, 73 (1984).
[13] R. P. Hememger, J. Chem. Phys. **66**, 1795 (1977).
[14] J. S. Briggs and A. Herzenberg, Mol. Phys. **21**, 865 (1971).
[15] Y. Won, R. Lagos, and R. Friesner, J. Chem. Phys. **84**, 6567 (1986); R. E. Lagos and R. A. Friesner, *ibid.* **81**, 5899 (1084).
[16] P. O. J. Scherer and S. F. Fischer, Chem. Phys. **86**, 269 (1984).
[17] J. Grad, G. Hernandez, and S. Mukamel, Phys. Rev. A **37**, 3838 (1988).
[18] H. Haken and G. Strobl, Z. Phys. **262**, 135 (1973).
[19] F. C. Spano and S. Mukamel, J. Chem. Phys. **91**, 683 (1989).
[20] N. N. Bogoliubov and S. V. Tyablikov, DAN SSSR **126**, 53 (1959).
[21] A. S. Davydov, in *Theory of Molecular Excitons* (Plenum, New York, 1971).
[22] F. C. Spano, J. R. Kuklinski, and S. Mukamel, Phys. Rev. Lett. **65**, 211 (1990).
[23] (a) A. I. Zaitsev, V. A. Malyshev, and E. D. Trifinov, Sov. Phys. JETP **57**, 275 (1983); (b) Y. C. Lee and P. S. Lee, Phys. Rev. B **10**, 344 (1974).
[24] H. Risken, *The Fokker–Planck Equation* (Springer, Berlin, 1984).
[25] S. Mukamel, D. S. Franchi, and R. F. Loring, Chem. Phys. **128**, 99 (1988).
[26] H. Fidder, J. Knoester, and D. A. Wiersma, Chem. Phys. Lett. **171**, 529 (1990).
[27] H. P. Dorn and A. Muller, J. Appl. Phys. B**43**, 167 (1987).
[28] H. Steil, S. Daehne, and K. Teuchner, J. Lumin. **39**, 351 (1988).
[29] V. Sundstrom, T. Gillbro, R. A. Gadonas, and A. Piskarskas, J. Chem. Phys. **89**, 2754 (1988).
[30] D. V. Brumbaugh, A. A. Muenter, W. Knox, G. Mourau, and B. Wittmershaus, J. Lumin. **32**, 783 (1984).